



*Supplement of*

## **Validation of a new global irrigation scheme in the land surface model ORCHIDEE v2.2**

**Pedro Felipe Arboleda-Obando et al.**

*Correspondence to:* Pedro Felipe Arboleda-Obando ([pedro.arboleda\\_obando@upmc.fr](mailto:pedro.arboleda_obando@upmc.fr))

The copyright of individual parts of the supplement might differ from the article licence.

## Supplement S1

5 This section shows volumes of water withdrawal for irrigation and of ET increase from ORCHIDEE and AQUASTAT for 1998-2002, as well as the irrigation rate (Sacks et al., 2009) in Fig. S1. Figures S2 and S3 show difference between Irr and NoIrr for additional variables, including energy terms. Figure S4 shows basins included in the analysis of the effect of the new irrigation module, and the corresponding discharge stations. Figure S5 shows the fraction of irrigated paddy rice, with a focus on Southeast Asia. S6 shows the irrigated area for both datasets used on the simulations, HID and LUH2. Fig. S7 shows the spatial distribution of ET bias compared to FLUXCOM, and zonal average values for simulated and observed datasets, and S8 shows the same information (bias modelling compared to LAI3g and zonal average values) for LAI.

Fig. S9 presents the irrigation bias by class of irrigated area, and for class of the ratio of irrigated area to total crop and grass soil column, using outputs from the long simulations. This figure also depicts the irrigation bias and irrigation rate by class of irrigation area and 'beta' parameter value, using outputs from the short simulations used in the sensitivity analysis and tuning process. Fig. S10 shows the map of soil texture as used by ORCHIDEE, and the corresponding map of field capacity SM, for areas with irrigated areas around year 2000. Finally, Fig. S11 shows the irrigation bias between simulation Irr and Sacks et al., 2009 dataset, in %, and the map of irrigation efficiency (ratio of ET increase to water withdrawal) by country.

We also present four tables. Table S1 shows goodness-of-fit metrics for ORCHIDEE discharge values and observed values from GRDC selected stations. We use four metrics: relative bias (equation 1), the relative change of amplitude of average monthly values (equation 2), the Pearson's correlation coefficient  $r$  (equation 3, (Helsel and Hirsch, 1992) and Kling-Gupta Efficiency KGE (equation 4, (Gupta et al., 2009; Kling et al., 2012)).

30

$$B = \frac{\sum_{i=1}^n (S_i - O_i)}{\sum_{i=1}^n (O_i)} \times 100 \quad (1)$$

$$RelAmp = \frac{\max (S_j)_{j=1,12} - \min (S_j)_{j=1,12}}{\max (O_j)_{j=1,12} - \min (O_j)_{j=1,12}} \times 100 \quad (2)$$

$$r = \frac{\sum_{i=1}^n (S_i - \bar{S})(O_i - \bar{O})}{\sqrt{\sum_{i=1}^n (S_i - \bar{S})^2} \sqrt{\sum_{i=1}^n (O_i - \bar{O})^2}} \quad (3)$$

$$KGE = 1 - ED = 1 - \sqrt{(r - 1)^2 + \left(\frac{\sigma_s}{\sigma_o} - 1\right)^2 + \left(\frac{\mu_s}{\mu_o} - 1\right)^2} \quad (4)$$

35

Here S and O represents simulated and observed values, respectively, n represents the monthly values from the time-series, j represents one of 12 the months in a year,  $\sigma$  represents the standard deviation, and  $\mu$  represents the average value, with indices s and o indicating simulated or observed time series.

40

In table S2 we show the sum of the capacity of dams used for irrigation. We also present the average values at large river basin for irrigated fraction and irrigated paddy fraction, and the bias of evapotranspiration and irrigation. In table S3 we present trends on TWSA from our simulations and from GRACE datasets, the trends of the differences between simulations and GRACE, and the depletion estimates from (Wada et al., 2012). Finally, in table S4 we show the field capacity soil moisture and the saturated soil moisture (porosity) by soil texture, and the the theoretical maximum ‘beta’ by texture, i.e. the ratio of field capacity soil moisture to saturated soil moisture.

45

### **Text on figures S7 and S8**

50

The NoIrr simulation has a negative bias distribution when we compare this simulation with Fluxcom dataset in irrigated areas (Fig. S7-a). The activation of irrigation in Irr does not correct the distribution of the bias. At the regional scale however, we observe that irrigation activation reduces ET bias, for instance in Southern Asia and India, and in Southern Europe and the Mediterranean (for instance Spain). In China

and the US, two irrigation hotspots, the reduction of the negative ET bias in the Irr simulation is small  
55 when we compare NoIrr and Irr simulations. Other areas pass from a negative to a positive bias between  
NoIrr and Irr simulations, for instance in Australia and South America.

The average zonal values at yearly, boreal winter, and boreal summer periods in the irrigated areas (Fig.  
S7-b) confirm that both simulations NoIrr and Irr underestimate ET when compared to the Fluxcom, with  
60 local exceptions. On the other hand, the activation of irrigation reduces the ET bias for Fluxcom and leads  
to an overestimation for Gleam. Seasonal effects do not change this general pattern, but the extension and  
localization of the bias reduction.

In the case of LAI, we observe that the NoIrr simulation has a positive bias when we compare it to the  
65 LAI3g dataset (Fig. S8-a) and that this positive bias increases in the Irr simulation, because irrigation  
enhances transpiration, thus photosynthesis and biomass production. In some areas of India, like the Indus  
river basin or Middle East, the activation of irrigation reduces a negative bias, but in general, the positive  
bias increases, for example in China.

70 The mean zonal values (Fig. S8-b) show that the LAI increase is mostly found in the northern hemisphere  
and in a small part of the southern hemisphere, roughly following the increase in ET. Seasonally, increases  
of LAI also are mostly found in the northern hemisphere. For example, in the boreal winter (austral  
summer, thus high biomass production in the southern hemisphere), just small latitude bands in the  
southern hemisphere show a statistically detected change due to activation of irrigation. This is probably  
75 led by the zonal distribution of irrigated areas, mostly concentrated in the northern hemisphere. Other  
factors like PFT distribution and local climate could also influence the small effect of irrigation on LAI  
in the southern hemisphere.

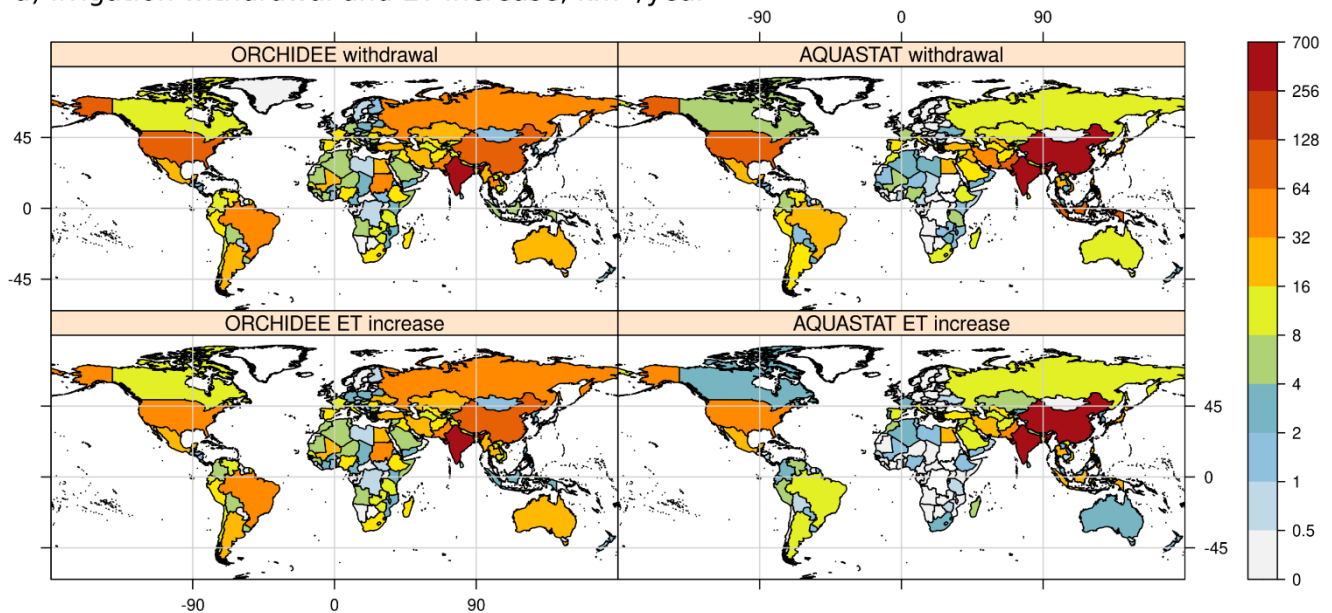
### **Text on figures S9 and S11**

In Fig. S9-a we show the irrigation bias by class of irrigated fraction. In comparison, Fig. S9-b shows the  
80 irrigation bias by class of irrigated surface over crop and grass soil column. While sparse irrigation in  
croplands could likely lead to overestimation in our model (see class 0-5 and 5-10 in S9-b), it is not always

the case. Also, underestimation in intensively irrigated areas is more important. In the second row, we show an additional analysis using outputs from the short simulations used in the sensitivity analysis and parameter tuning process. While Fig. S9-c shows that the increase of 'beta' will always induce an increase of irrigation rate, with no regard to irrigated area class, the effect of a higher 'beta' value on irrigation bias is different according to the class. For instance, for class 50-100, a higher 'beta' value in general decrease the irrigation bias, while for class 5-10, a 'beta' value of 1.4 will likely induce an overestimation of the irrigation and a 'beta' value of 0.6 will likely induce an underestimation.

90 In Fig. S11-a we can observe in one hand a strong overestimation in % (red). These areas depict a small irrigation rate (0.01 to 0.05 mm/d) that is strongly surpassed by the simulations, but the absolute value remains relatively small. On the other hand, we observe areas with a strong underestimation (blue). These areas show higher irrigation rates than the areas in red (over 0.1) and in general, fit well with regions where paddy rice is important. Irrigation efficiency map by country (in Fig. S11-b) show values over 95 100% in some countries. This high irrigation efficiency values mean that the crops increase ET by using a higher fraction of rainfall, even when there is not irrigation in the area. This is the result of suppressing part of the crop water stress, and lacking a specialized phenology module with crop stages like germination and harvesting. As crops are not harvested, even if there is not irrigation, there is more ET.

a) Irrigation withdrawal and ET increase, km<sup>3</sup>/year



b) Irrigation rates from Sacks et al., 2009, mm/d

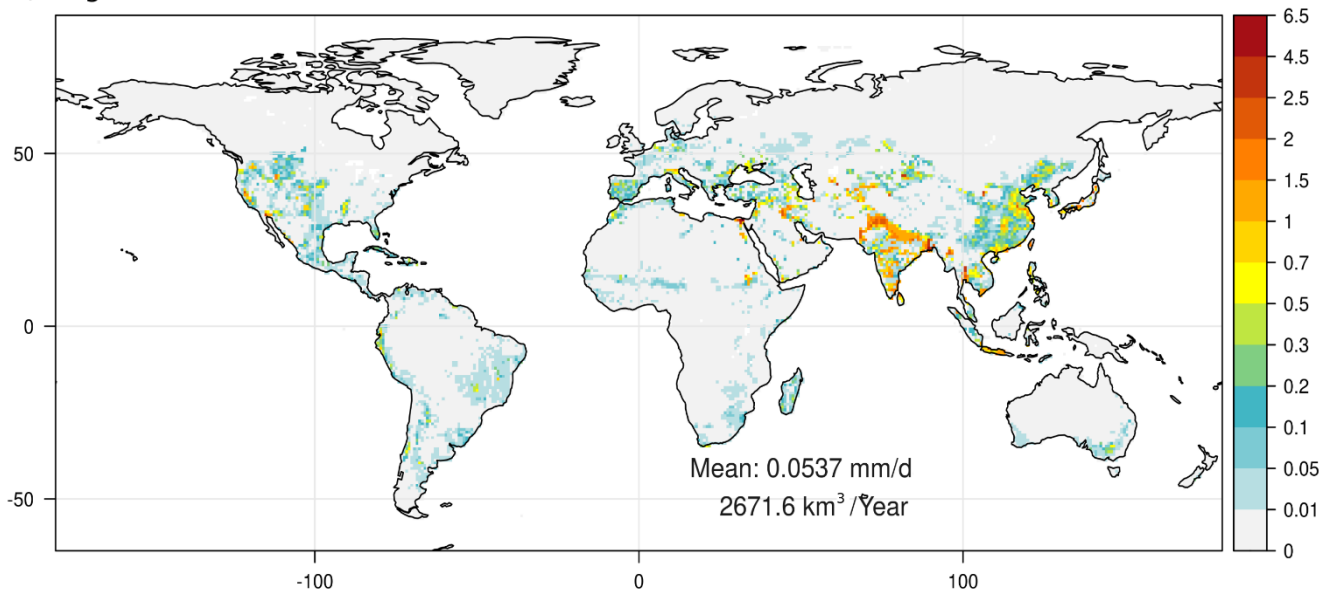
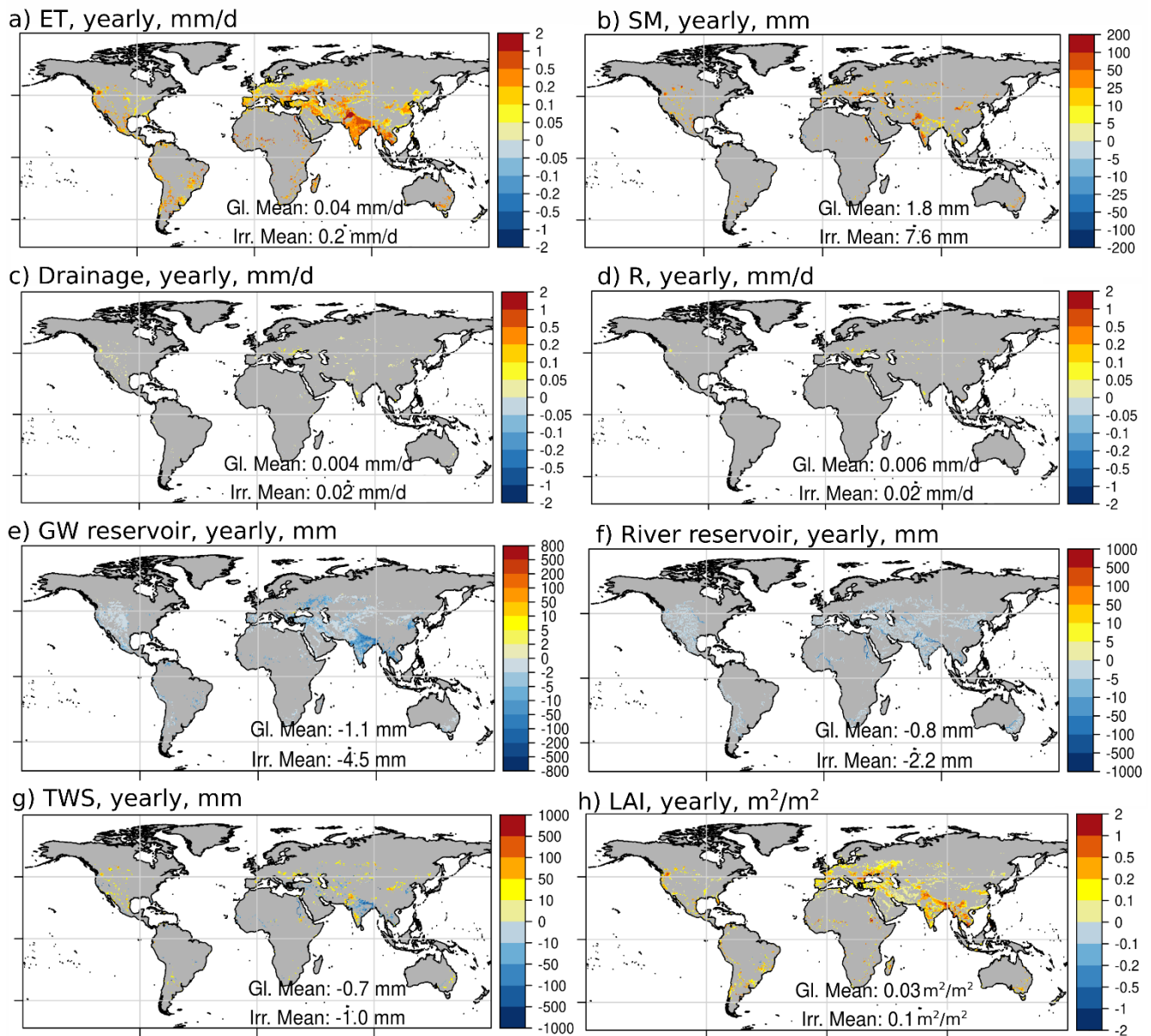
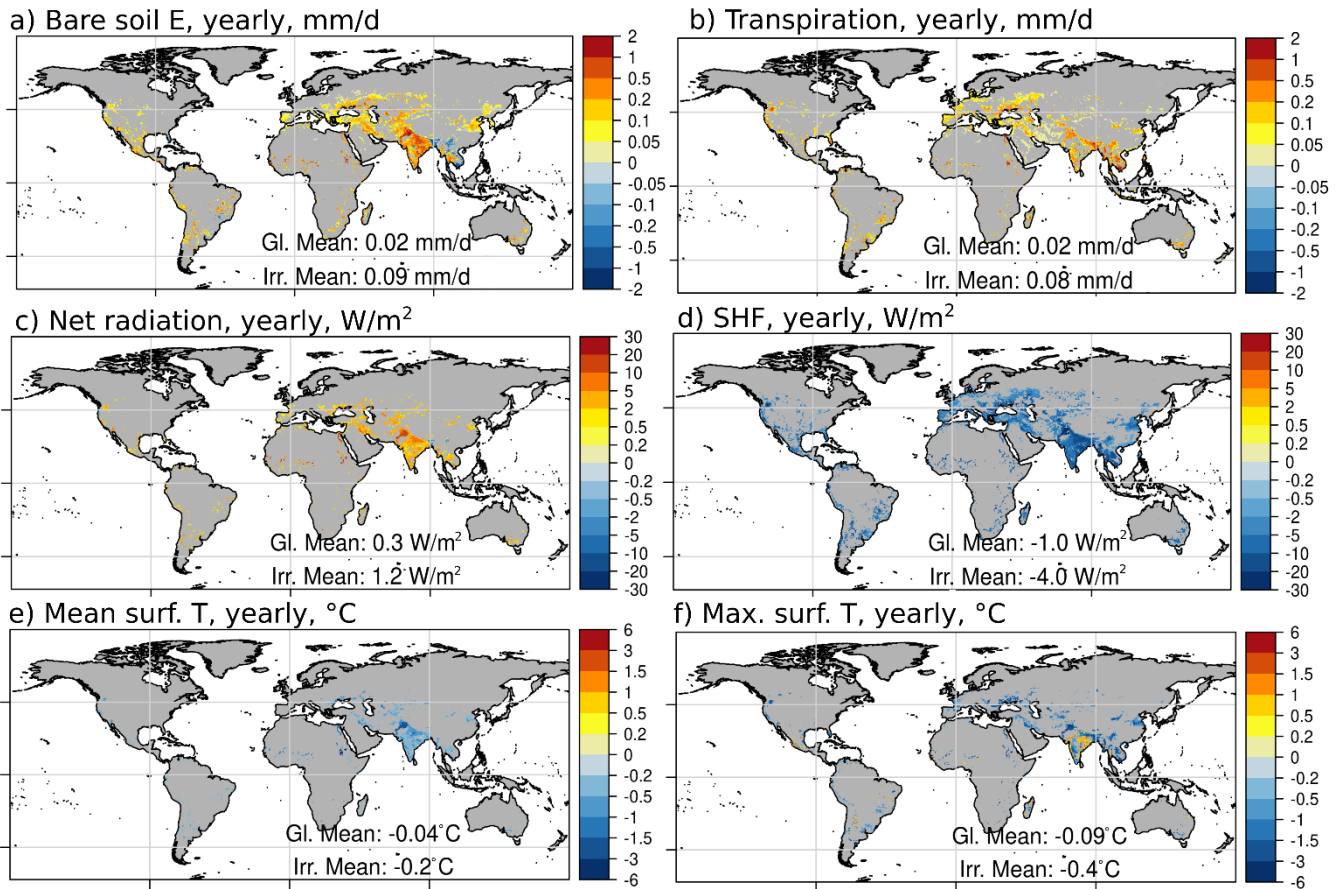


**Figure S.1 Volumes of water withdrawal for irrigation and ET increase (called irrigation requirement in AQUASTAT dataset) by country from ORCHIDEE (Irr simulation, average value for 1998-2002), and AQUASTAT (value around 2000), in km<sup>3</sup>/year (a). Irrigation rate from (Sacks et al., 2009) for year 2000, mm/d.**

105

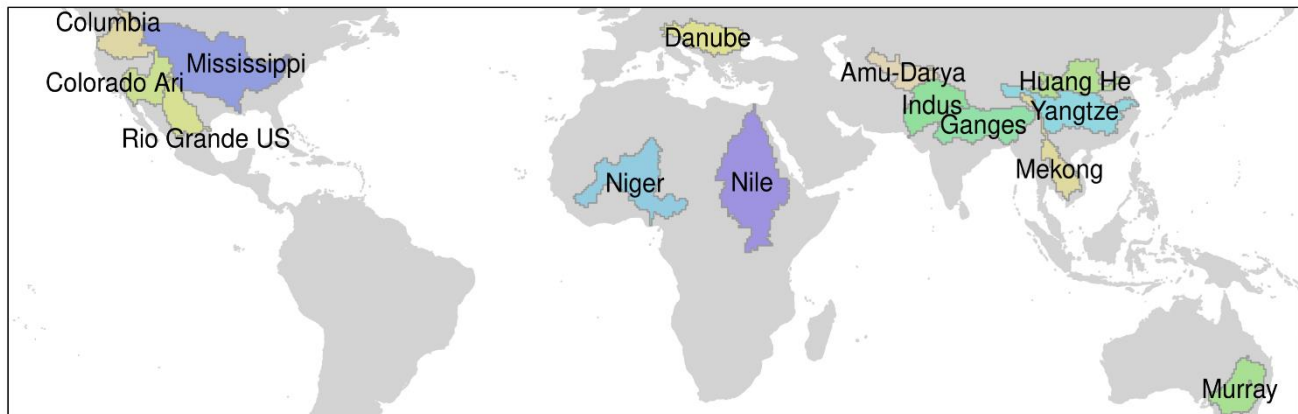


110 **Figure S2** Yearly average difference for 1980 - 2013 between Irr and NoIrr of ET, mm/d (a), SM, mm (b), drainage, mm/d (c), total runoff (R), mm/d (d), groundwater (GW) reservoir, mm (e), river reservoir, mm (f), TWS, mm (g), and LAI,  $m^2/m^2$  (h). Statistical significance of the mean differences is tested at each point with a Student's test ( $p = 0.05$ ). The areas with insignificant changes are left gray.



120 **Figure S3** Yearly average difference for 1980 - 2013 between Irr and NoIrr of bare soil E, mm/d (a), T, mm/d (b), net radiation  $W/m^2$  (c), SHF,  $W/m^2$  (d), mean surface temperature,  $^{\circ}C$  (e), and max. surface temperature,  $^{\circ}C$  (f). Statistical significance of the mean differences is tested at each point with a Student's test ( $p = 0.05$ ). The areas with insignificant changes are left gray.

### a) Basins



### b) Discharge stations

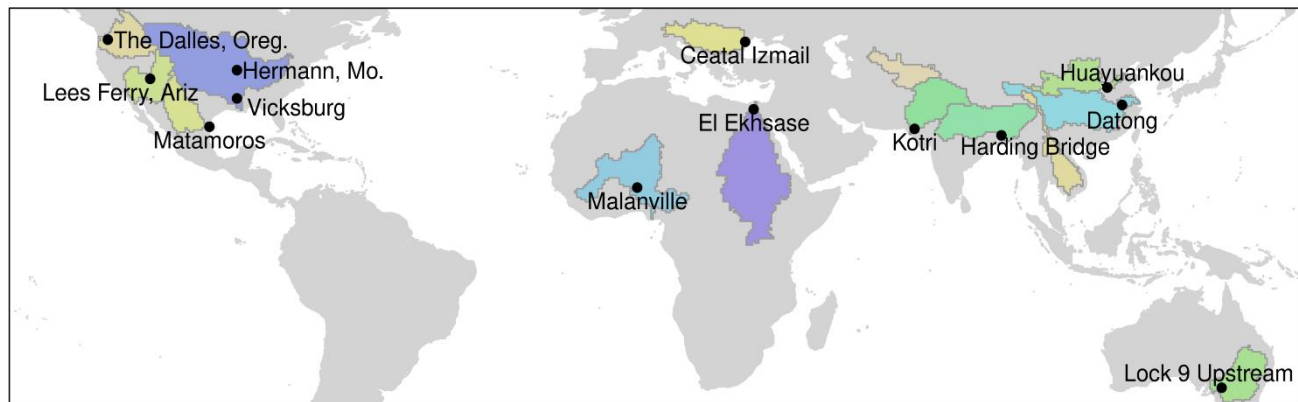
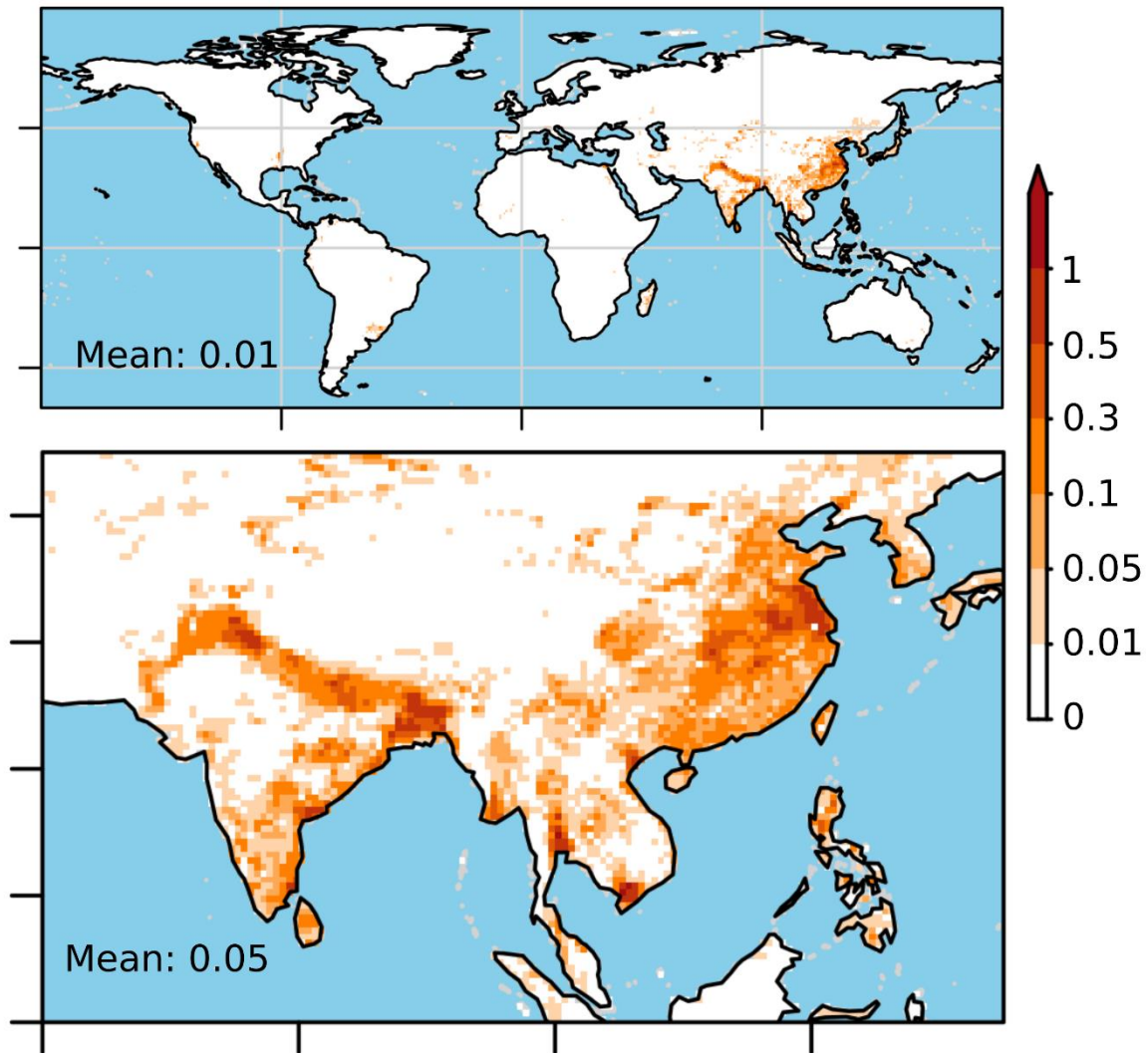
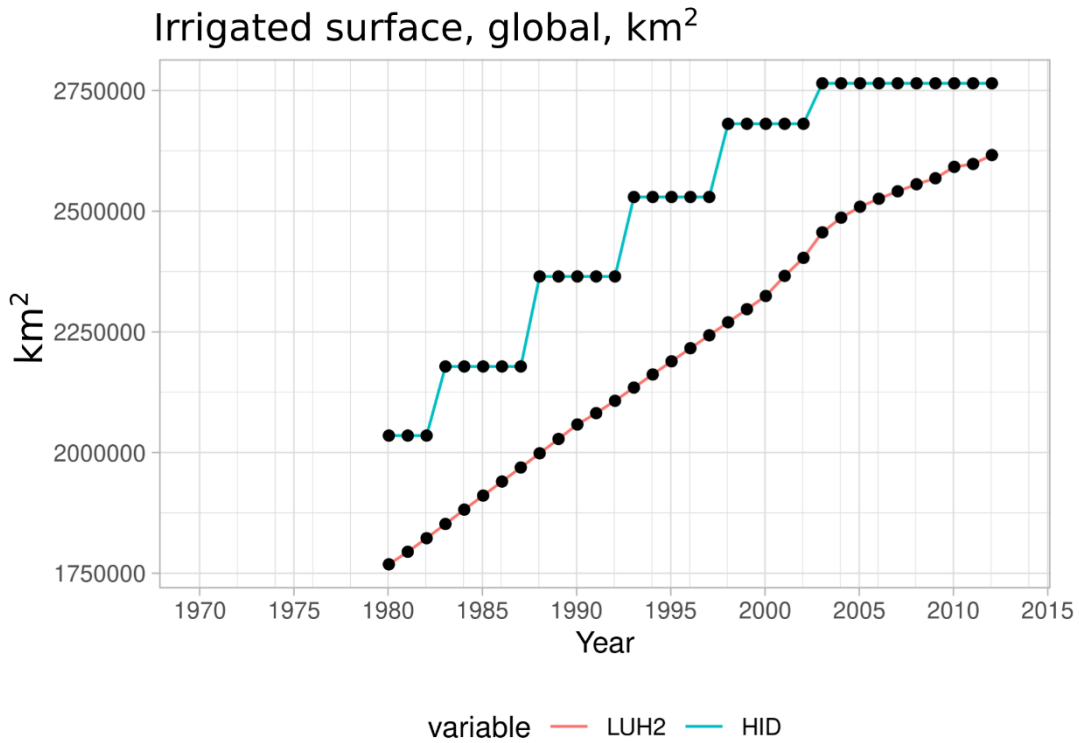


**Figure S4** Limits of large basins used in the regional analysis (a). Discharge stations used in the comparison with ORCHIDEE outputs (b).

## Fraction of irrigated paddy rice, and focus in Southeast Asia



135 **Figure S5** Fraction of irrigated paddy rice, and focus on Southeast Asia. Data comes from **MIRCA2000** (Portmann et al., 2010).

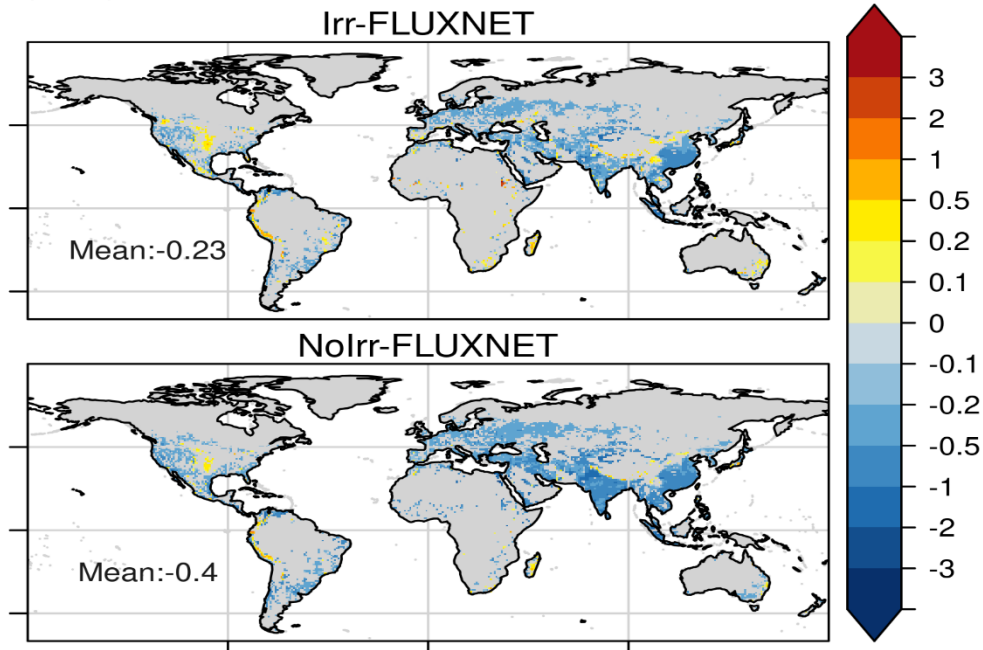


145

**Figure S6 Total irrigated surface in km<sup>2</sup>, for HID (Siebert et al., 2015) and LUH2 (Hurtt et al., 2020).**

150

a) ET bias, yearly (mm/d)



c) ET, zonal average in irrigated areas, mm/d

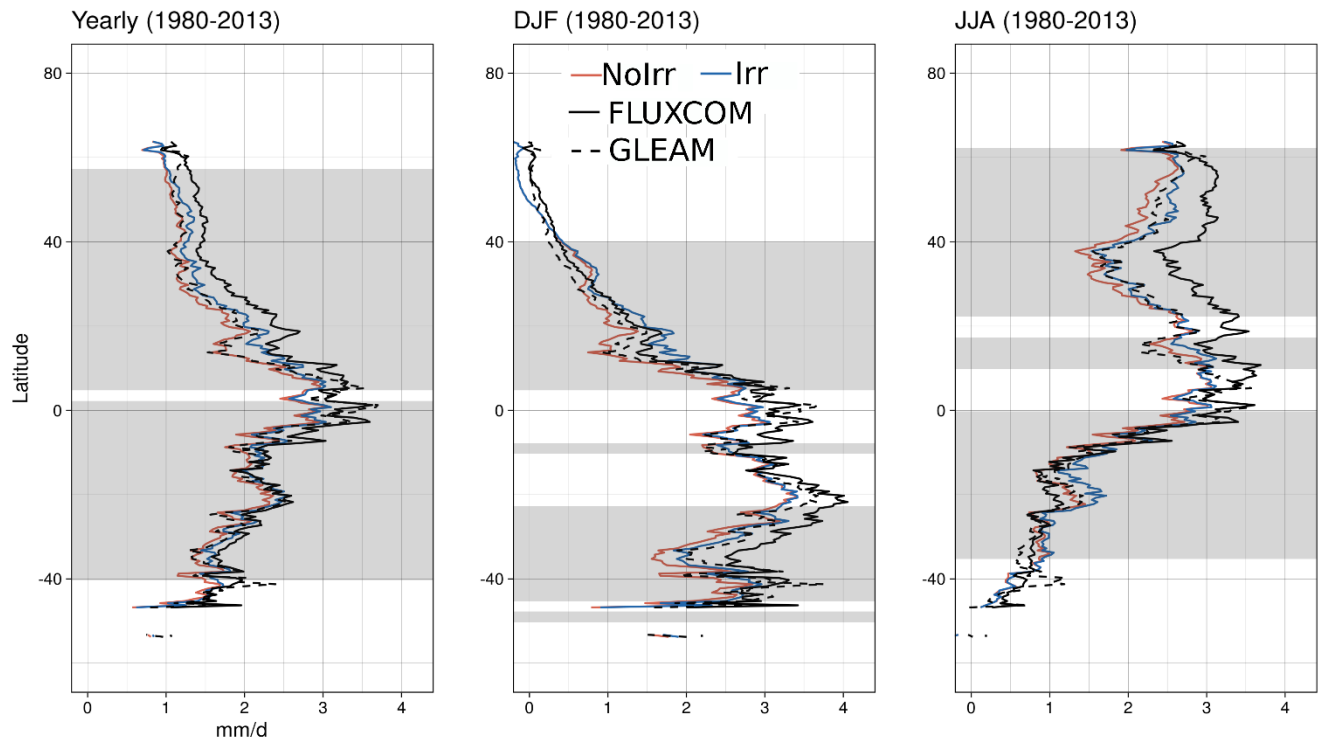
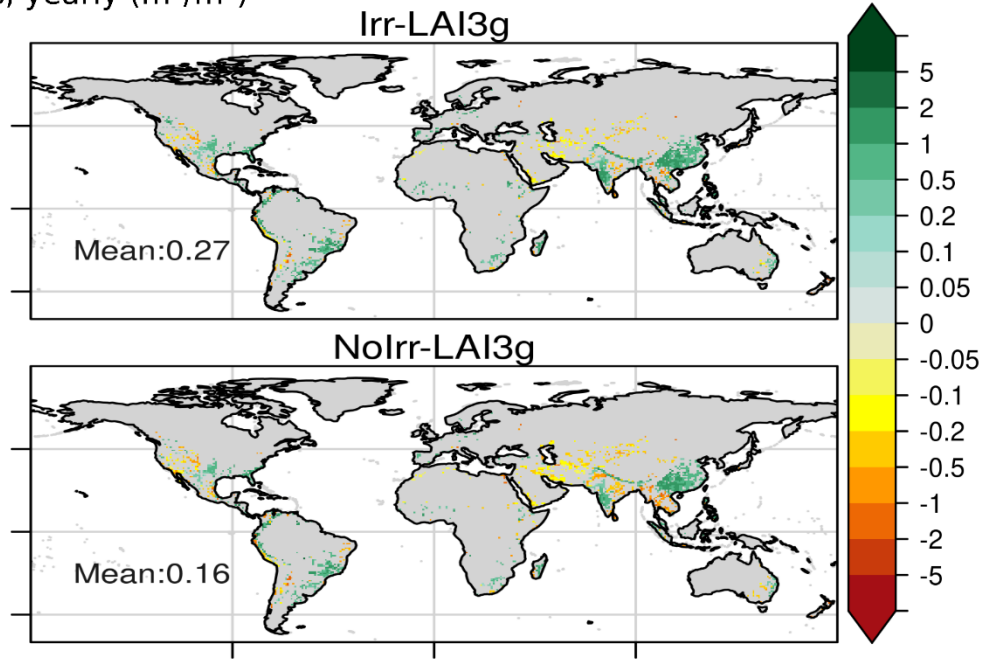


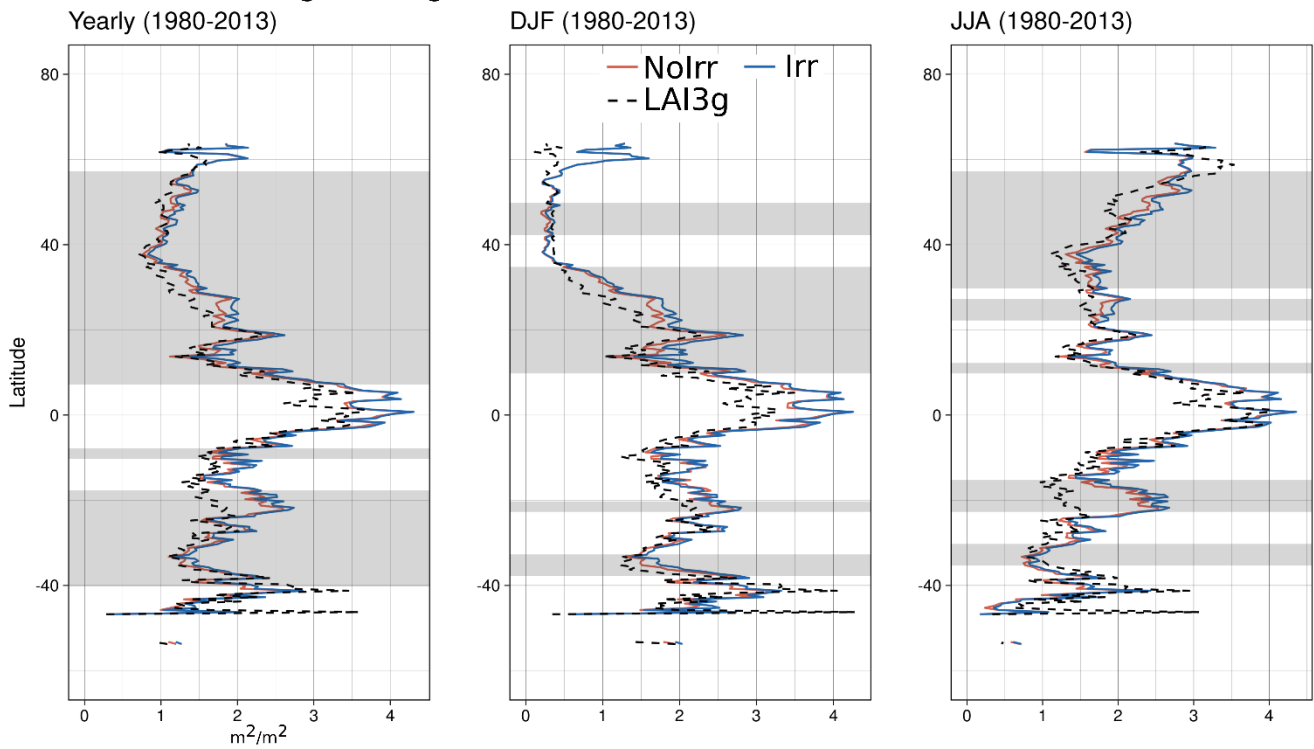
**Figure S7 Difference of yearly average values for 1980 - 2013 between NoIrr and Irr simulations, and Fluxcom (a) and for NoIrr and Irr simulations, for ET in mm/d. Statistical significance of the mean differences is tested at each point with a Student's test ( $p = 0.05$ ). The areas with insignificant changes or no irrigated fraction are left gray. Zonal average values of areas with irrigated fractions for yearly, boreal summer (JJA) and boreal winter (DJF) of ET for period 1980 - 2013 (b) in mm/d. Gray areas for zonal average values depict the latitudes with significant differences between Irr and NoIrr simulation, according to the Student t-test ( $p = 0.05$ ).**

160

a) LAI bias, yearly ( $\text{m}^2/\text{m}^2$ )



b) LAI, zonal average in irrigated areas,  $\text{m}^2/\text{m}^2$



165 **Figure S8 Difference of yearly average values for 1980 - 2013 between NoIrr and Irr simulations,**  
**and LAI3g (a) for LAI in  $m^2/m^2$ . Statistical significance of the mean differences is tested at each**  
**point with a Student's test ( $p = 0.05$ ). The areas with insignificant changes or no irrigated fraction**  
**are left gray. Zonal average values of areas with irrigated fractions for yearly, boreal summer (JJA)**  
**and boreal winter (DJF) of LAI for period 1980 - 2013 (b) in  $m^2/m^2$ . Gray areas for zonal average**  
170 **values depict the latitudes with significant differences between Irr and NoIrr simulation, according**  
**to the t-student test ( $p = 0.05$ ).**

175

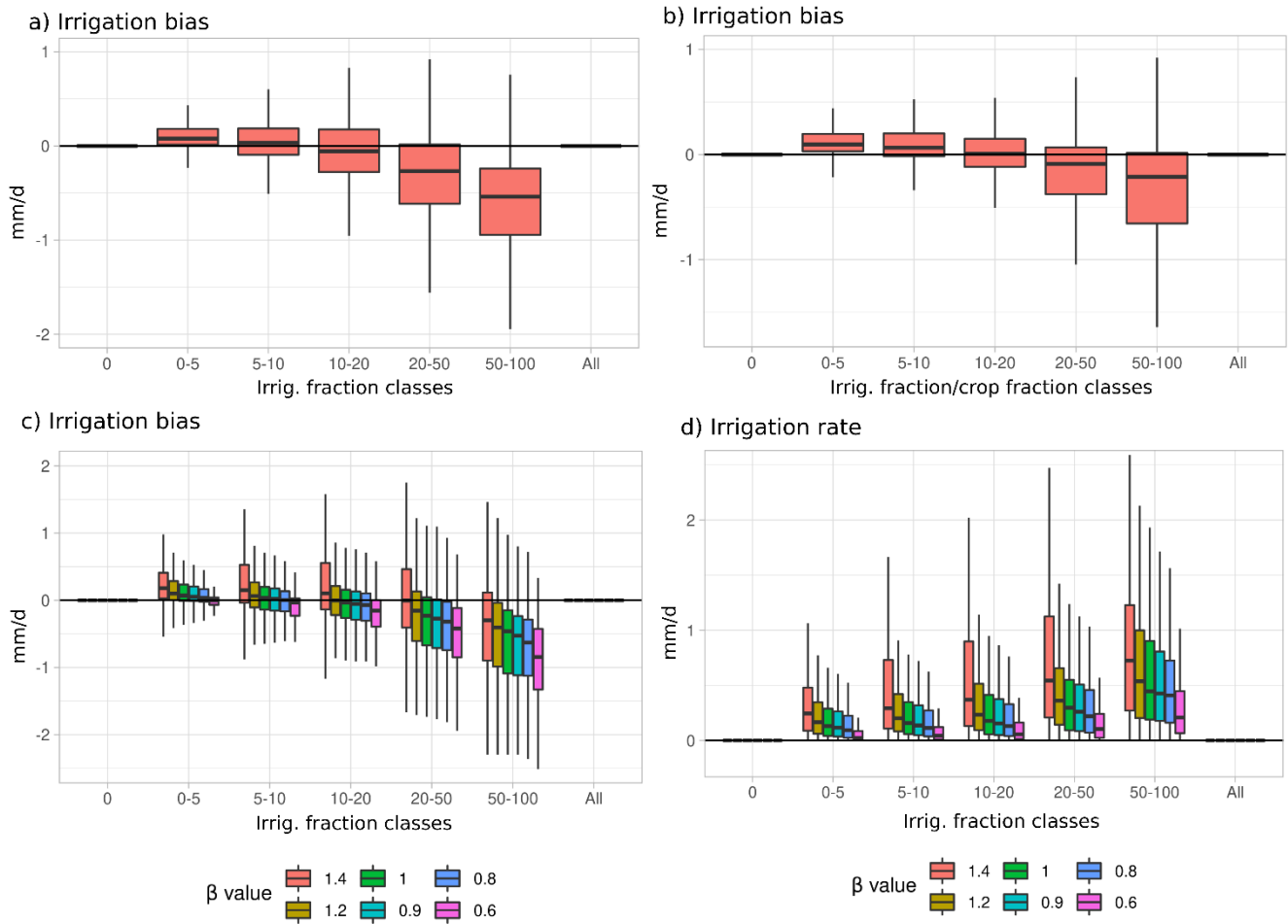
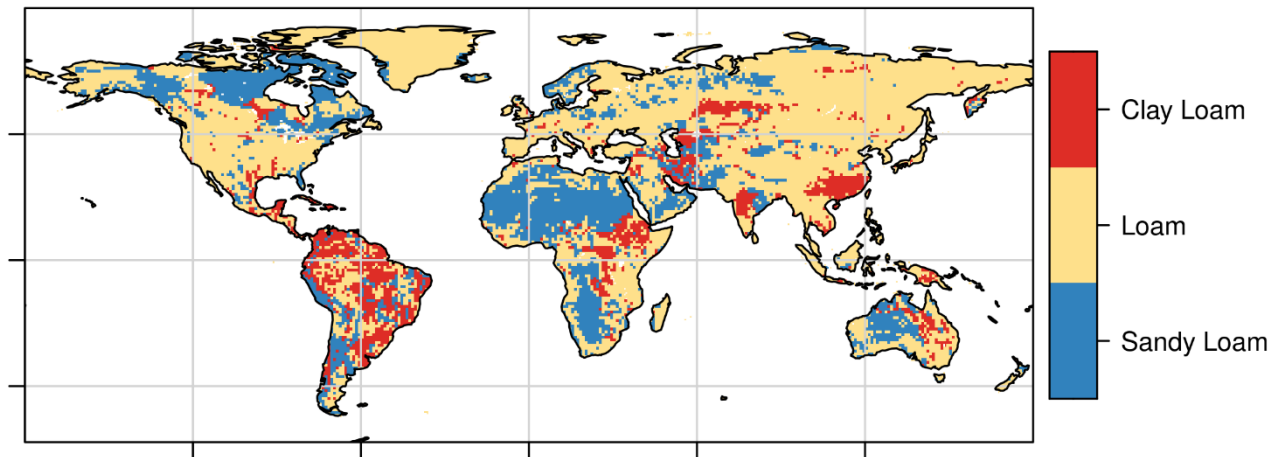


**Figure S9 Use of factor analysis against irrigation bias. Irrigation rate bias against data from Sacks et al. (2009), as a function of irrigated fraction classes (a) and classes of the ratio of irrigated fraction and crops and grasses soil column fraction (b). Both plots use data from the Irr simulation for 2000.**

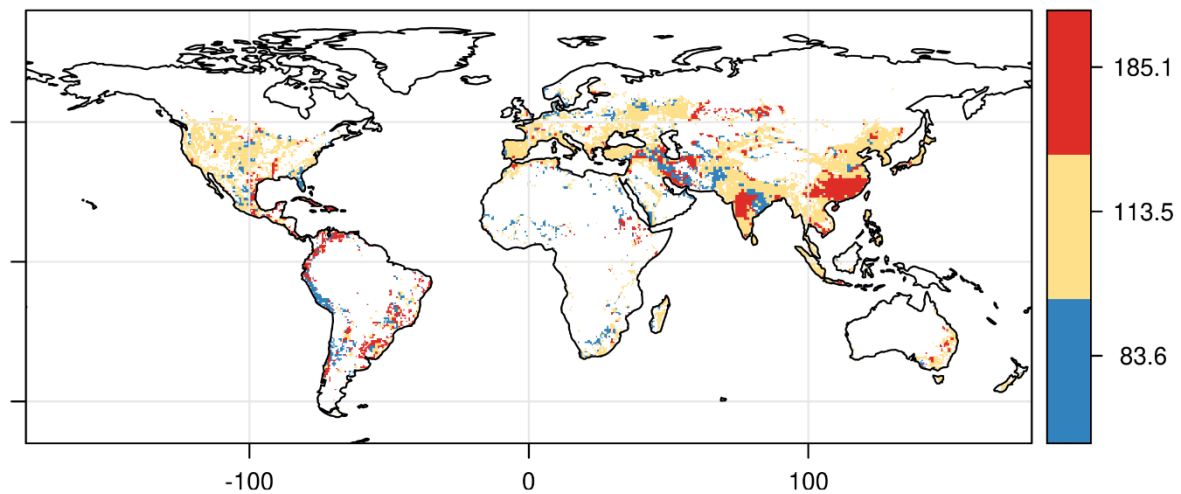
180 **Irrigation rate bias against data from Sacks et al. (2009), as a function of irrigated fraction classes and ‘beta’ parameter values (c). Irrigation rate as a function of irrigated fraction classes and ‘beta’ parameter values (d). Both plots (c) and (d) use data from short simulations used for the sensitivity analysis and the tuning parameter analysis, for 2000.**

185

a) Soil texture map used by ORCHIDEE

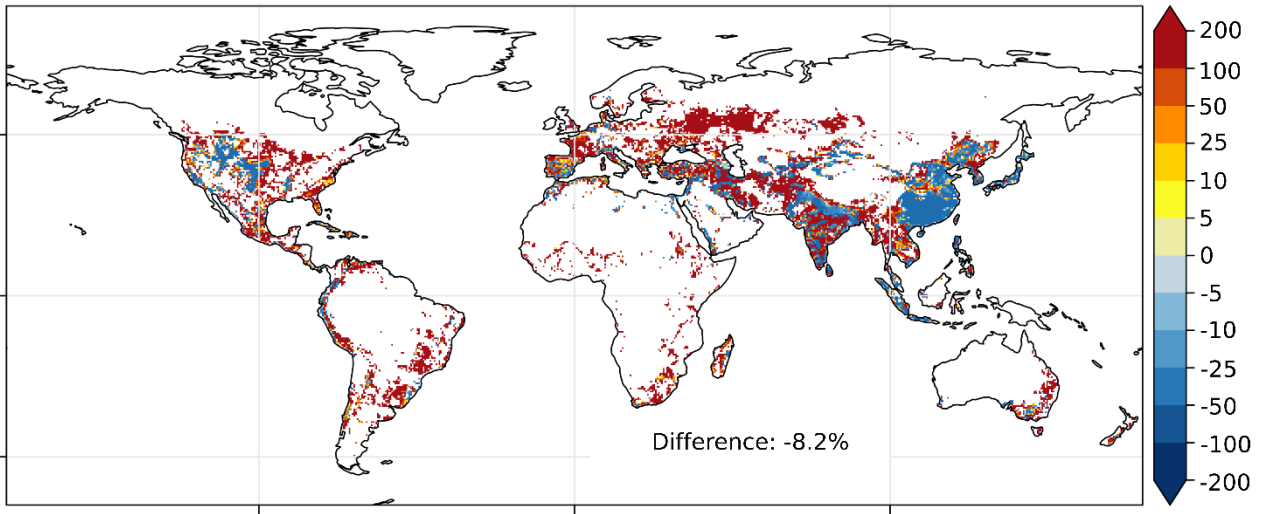


b) Field capacity SM in defined root zone, in  $\text{kg/m}^2$

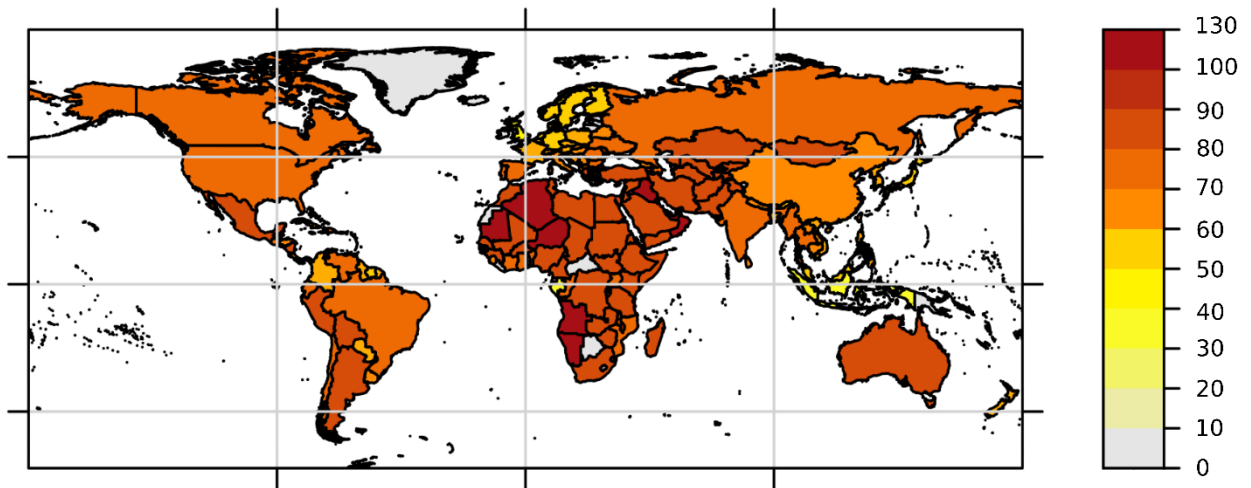


190 **Figure S10 Soil texture map used by ORCHIDEE from Zobler (a) and field capacity soil moisture in the root zone defined according to the new irrigation scheme, in  $\text{kg/m}^2$  or mm. Both maps are at the simulation resolution ( $0.5^\circ \times 0.5^\circ$ ). White in (b) means that there is no irrigated fraction in the gridcell, according to HID map for year 2000.**

a) Difference on irrigation, Irr - Sacks et al., 2009, (1998-2002) , in %



b) Irrigation efficiency by country, in %



200 **Figure S11 Difference in % in water withdrawal between Irr (yearly average 1998-2002) and dataset from Sacks et al., 2009 (a). Irrigation efficiency from Irr simulation (yearly average 1998-2002) as the ratio of increase of evapotranspiration to irrigation withdrawal (b).**

205 **Table S1 Goodness-of-fit metrics for ORCHIDEE discharge values and GRDC selected stations. RelAmpli stands for relative change on amplitude, r for Pearson correlation coefficient, KGE for Kling-Gupta efficiency.**

Metric River@Station	GWF-REF (%)	Bias %		RelAmpli%		r		KGE	
		Nolrr	Irr	Nolrr	Irr	Nolrr	Irr	Nolrr	Irr
Indus @ Kotri	-90.79								
Rio Grande (MX) @ Matamoros	-81.43	6387.44	1104.72	8349.66	2306.7	0.12	0.13	-71.71	-17.76
Yellow River @ Huayuankou	-67.66	-3.93	-68.93	-40.77	-65.64	0.54	0.2	0.39	-0.18
Amu-Darya @ Chatly	-65.8								
Murray @ Lock 9 Upstream	-53.31	832.45	335.41	196.11	84.54	0.47	0.48	-8.13	-3.53
Colorado (Ariz.) @ Lees Ferry, Ariz	-42.35	-46.84	-69.36	78.69	134.17	0.08	0.01	-0.03	-0.21
Nile @ El Ekhsase	-33.43	794.01	495.14	1736.17	1949.26	-0.27	-0.31	-22.15	-23.15
Columbia @ The Dalles, Oreg.	-26.54	-41.43	-56.97	8.47	25.68	0.8	0.69	0.54	0.34
Ganges-Brahmaputra @ Harding Bridge	-25.59	82.23	35.6	7.07	18.49	0.77	0.75	0.15	0.55
Missouri @ Hermann, Mo.	-24.08	2.24	-22.38	-43.27	-54.33	0.59	0.69	0.59	0.61
Danube @ Ceatal Izmail	-16.76	10.73	-7.83	29.72	23.96	0.67	0.83	0.63	0.66
Niger @ Malanville	-9.05	506.67	451.77	360.38	373.96	0.58	0.61	-5.25	-4.85
Mississippi @ Vicksburg	-5.08	-7.23	-11.94	-54	-47.65	0.62	0.69	0.43	0.49
Yangtze @ Datong	-2.08	-9.99	-11.87	-36.72	-37.98	0.88	0.88	0.64	0.63

**Table S2 Dams capacity used for irrigation, irrigated fraction and paddy irrigated fraction, ET and irrigation bias at large river basin scale.**

Basin	Dams for irrig. 10 <sup>6</sup> m <sup>3</sup>	Irrigated fraction	Irrigated paddy fraction	Nolrr- Gleam mm/d	Irr- Gleam mm/d	Nolrr- Fluxcom mm/d	Irr- Fluxcom mm/d	Irrigation bias mm/d
Nile	173411	0.010	0.001	0.015	0.114	-0.508	-0.361	0.044
Indus	44828	0.190	0.052	0.079	0.470	-0.724	-0.323	-0.043
Ganges	32589	0.178	0.080	-0.016	0.280	-0.364	-0.068	-0.124
Amu-Darya	25500	0.072	0.002	-0.010	0.161	-0.611	-0.440	-0.073
Columbia	22713	0.044	0.000	-0.343	-0.245	-0.246	-0.148	-0.038
Rio Grande US	19478	0.021	0.000	0.095	0.163	-0.208	-0.140	0.036
Yangtze	19186	0.082	0.091	-0.216	-0.188	-0.370	-0.342	-0.102
Murray	17484	0.021	0.001	-0.006	0.087	-0.162	-0.069	0.067
Mississippi	16915	0.037	0.002	0.110	0.142	-0.079	-0.047	-0.030
Niger	16400	0.001	0.001	0.009	0.055	-0.485	-0.427	0.023
Colorado Ari	6355	0.021	0.000	0.000	0.053	-0.327	-0.273	-0.031
Mekong	4379	0.027	0.030	-0.265	-0.068	-0.431	-0.234	0.103
Huang He	2337	0.078	0.021	0.080	0.163	-0.061	0.022	-0.042
Danube	1762	0.037	0.000	-0.044	0.080	-0.433	-0.308	0.120

215

220

**Table S3 Trends of Total Water Store (TWS) values from simulations (NoIrr and Irr) and from the average of GRACE datasets by country, difference between simulated trends and GRACE, and comparison with depletion values from (Wada et al., 2012).**

id	Country	NoIrr km <sup>3</sup> /y	Irr km <sup>3</sup> /y	GRACE km <sup>3</sup> /y	NoIrr-GRACE km <sup>3</sup> /y	Irr-GRACE km <sup>3</sup> /y	Depletion from (Wada et al., 2012) km <sup>3</sup> /y
1	India	10.42	8.03	-11.10	27.02	28.46	71.00
2	United States	3.70	3.51	-64.58	69.71	65.08	32.00
3	China	24.57	24.49	-15.16	38.16	38.36	22.00
4	Pakistan	4.78	4.58	1.43	3.28	2.76	37.00
5	Iran	-0.18	-0.28	-20.40	19.93	20.29	27.00
6	Mexico	1.62	1.35	-0.72	3.39	2.93	11.00
7	Saudi Arabia	-1.02	-0.98	-15.71	15.00	15.00	15.00
8	Russian Federation	7.92	7.67	-70.76	69.62	60.27	1.50
9	Italy	0.40	0.42	-0.59	0.86	0.97	2.30
10	Turkey	0.12	0.16	-3.73	3.81	3.61	2.40
11	Uzbekistan	-0.83	-0.79	-2.69	1.81	1.89	4.00
12	Egypt	-0.88	-0.89	-4.49	3.65	3.32	3.00
13	Bulgaria	-0.01	-0.04	-0.63	0.57	0.56	2.00
14	Spain	-0.15	-0.14	0.10	0.33	0.30	1.70
15	Argentina	-11.43	-11.10	-34.76	25.09	25.23	0.90
16	Libya	-1.35	-1.34	-5.70	4.44	4.22	3.10
17	Ukraine	0.71	0.63	-4.69	6.16	5.95	0.30
18	Romania	0.78	0.43	-1.44	1.99	1.82	1.30
19	Kazakhstan	-1.08	-0.79	-18.33	19.06	19.30	2.00
20	South Africa	0.64	0.70	3.92	-3.23	-3.19	1.50
21	Algeria	1.07	1.07	-3.37	4.68	4.90	1.70
22	Greece	-0.17	-0.18	-0.21	0.11	0.10	0.34
23	Morocco	1.09	1.04	1.63	-0.26	-0.19	1.60
24	Australia	17.46	17.78	25.21	-3.25	-4.16	1.00
25	Tajikistan	-0.31	-0.31	-1.08	0.68	0.42	1.20
26	Yemen	-0.11	-0.11	-1.26	1.13	1.15	0.90

27	Turkmenistan	-0.77	-0.70	0.00	-0.86	-0.85	1.25
28	Syria	-0.46	-0.42	-2.32	2.03	2.03	1.23
29	United Arab Emirates	0.10	0.10	-0.19	0.33	0.33	1.18
30	Tunisia	-0.17	-0.16	-0.67	0.54	0.49	0.65
31	Peru	-6.17	-6.20	-4.44	-3.01	-3.74	0.32
32	Bolivia	5.85	5.79	0.61	4.95	5.09	0.25
33	Israel	-0.06	-0.05	-0.13	0.08	0.09	0.38
34	Kyrgyzstan	-0.52	-0.47	-0.78	0.52	0.45	0.31
35	Jordan	-0.12	-0.12	-0.97	0.89	0.85	0.22
36	Mauritania	0.94	0.94	1.12	-0.38	-0.45	0.36
37	Oman	1.08	1.08	-0.69	1.88	1.83	0.20
38	Kuwait	-0.06	-0.06	-0.05	-0.01	0.00	0.25
39	Qatar	-0.01	-0.01	-0.05	0.04	0.04	0.15

230 **Table S4 Parameters for soil textures used in ORCHIDEE.  $\theta_s$  is saturated soil moisture and  $\theta_{fc}$  is the field capacity soil moisture, in volumetric content.  $\beta_{max}$  is the theoretical maximum  $\beta$  value that can be used, where  $\beta = \theta_s/\theta_{fc}$ , so the target soil moisture ( $\beta \times \theta_{fc}$ ) does not surpass saturated conditions.**

Parameter	Sandy Loam	Loam	Clay Loam
$\theta_s$ (m <sup>3</sup> /m <sup>3</sup> )	0.41	0.43	0.41
$\theta_{fc}$ (m <sup>3</sup> /m <sup>3</sup> )	0.1218	0.1654	0.2697
$\beta_{max}$ (-)	3.4	2.6	1.5

## References

- 235 Gupta, H. V, Kling, H., Yilmaz, K. K., and Martinez, G. F.: Decomposition of the mean squared error  
and NSE performance criteria : Implications for improving hydrological modelling, *J. Hydrol.*, 377, 80–  
91, <https://doi.org/10.1016/j.jhydrol.2009.08.003>, 2009.
- Helsel, D. R. and Hirsch, R. M.: Statistical methods in water resources, *Stat. methods water Resour.*,  
<https://doi.org/10.2307/1269385>, 1992.
- 240 Hurtt, G. C., Chini, L., Sahajpal, R., Frohling, S., Bodirsky, B. L., Calvin, K., Doelman, J. C., Fisk, J.,  
Fujimori, S., Klein Goldewijk, K., Hasegawa, T., Havlik, P., Heinemann, A., Humpenöder, F., Jungclaus,  
J., Kaplan, J. O., Kennedy, J., Krisztin, T., Lawrence, D., Lawrence, P., Ma, L., Mertz, O., Pongratz, J.,  
Popp, A., Poulter, B., Riahi, K., Shevliakova, E., Stehfest, E., Thornton, P., Tubiello, F. N., van Vuuren,  
D. P., and Zhang, X.: Harmonization of global land use change and management for the period 850–2100  
(LUH2) for CMIP6, *Geosci. Model Dev.*, 13, 5425–5464, <https://doi.org/10.5194/gmd-13-5425-2020>,  
245 2020.
- Kling, H., Fuchs, M., and Paulin, M.: Runoff conditions in the upper Danube basin under an ensemble of  
climate change scenarios, *J. Hydrol.*, 424–425, 264–277, <https://doi.org/10.1016/j.jhydrol.2012.01.011>,  
2012.
- 250 Portmann, F. T., Siebert, S., and Döll, P.: MIRCA2000-Global monthly irrigated and rainfed crop areas  
around the year 2000: A new high-resolution data set for agricultural and hydrological modeling, *Global  
Biogeochem. Cycles*, 24, n/a-n/a, <https://doi.org/10.1029/2008GB003435>, 2010.
- Sacks, W. J., Cook, B. I., Buening, N., Levis, S., and Helkowski, J. H.: Effects of global irrigation on  
the near-surface climate, *Clim. Dyn.*, 33, 159–175, <https://doi.org/10.1007/s00382-008-0445-z>, 2009.
- 255 Siebert, S., Kummu, M., Porkka, M., Döll, P., Ramankutty, N., and Scanlon, B. R.: A global data set of  
the extent of irrigated land from 1900 to 2005, *Hydrol. Earth Syst. Sci.*, 19, 1521–1545,  
<https://doi.org/10.5194/hess-19-1521-2015>, 2015.
- Wada, Y., Van Beek, L. P. H., and Bierkens, M. F. P.: Nonsustainable groundwater sustaining irrigation:  
A global assessment, *Water Resour. Res.*, 48, <https://doi.org/10.1029/2011WR010562>, 2012.